JGR Planets

RESEARCH ARTICLE

10.1029/2020JE006569

Formation of Tridymite and Evidence for a Hydrothermal History at Gale Crater, Mars

A. S. Yen[1], R. V. Morris[2], D. W. Ming[2], S. P. Schwenzer[3], B. Sutter[2], D. T. Vaniman[4], A. H. Treiman[5], R. Gellert[6], C. N. Achilles[7], J. A. Berger[2], D. F. Blake[8], N. I. Boyd[6], T. F. Bristow[8], S. Chipera[9], B. C. Clark[10], P. I. Craig[4], R. T. Downs[11], H. B. Franz[7], T. Gabriel[12], A. C. McAdam[7], S. M. Morrison[13], C. D. O'Connell-Cooper[14], E. B. Rampe[2], M. E. Schmidt[15], L. M. Thompson[14], and S. J. VanBommel[16]

[1]Jet Propulsion Laboratory, California Institute of Technology, Pasadena, CA, USA, [2]Johnson Space Center, NASA, Houston, TX, USA, [3]School of Environment, Earth & Ecosystem Sciences, The Open University, Milton Keynes, UK, [4]Planetary Science Institute, Tucson, AZ, USA, [5]Lunar and Planetary Institute, Houston, TX, USA, [6]Department of Physics, University of Guelph, Guelph, ON, USA, [7]Goddard Space Flight Center, NASA, Greenbelt, MD, USA, [8]Ames Research Center, NASA, Moffett Field, CA, USA, [9]Chesapeake Energy Corporation, Oklahoma City, OK, USA, [10]Space Science Institute, Boulder, CO, USA, [11]Department of Geosciences, University of Arizona, Tucson, AZ, USA, [12]School of Earth and Space Exploration, Arizona State University, Tempe, AZ, USA, [13]Earth and Planets Laboratory, Carnegie Institution, Washington, DC, USA, [14]Department of Earth Sciences, University of New Brunswick, Fredericton, NB, Canada, [15]Department of Earth Sciences, Brock University, St. Catharines, ON, Canada, [16]Department of Earth and Planetary Sciences, Washington University in St. Louis, St. Louis, MI, USA

Key Points:

- Chemical and mineralogical data from the Curiosity Mars rover suggest a history of hydrothermal alteration within Gale crater
- Silica-rich alteration halos and tridymite-bearing deposits exhibit similar chemical signatures, suggesting related formation processes
- We propose the in situ formation of tridymite through hydrothermal processes as an alternative to a detrital origin

Supporting Information:

- Supporting Information S1

Correspondence to:

A. S. Yen,
Albert.Yen@jpl.caltech.edu

Citation:

Yen, A. S., Morris, R. V., Ming, D. W., Schwenzer, S. P., Sutter, B., Vaniman, D. T., et al. (2021). Formation of tridymite and evidence for a hydrothermal history at Gale crater, Mars. *Journal of Geophysical Research: Planets*, *126*, e2020JE006569. https://doi.org/10.1029/2020JE006569

Received 11 JUN 2020
Accepted 2 DEC 2020

Abstract In August 2015, the Curiosity Mars rover discovered tridymite, a high-temperature silica polymorph, in Gale crater. The existing model for its occurrence suggests erosion and detrital sedimentation from silicic volcanic rocks in the crater rim or central peak. The chemistry and mineralogy of the tridymite-bearing rocks, however, are not consistent with silicic volcanic material. Using data from Curiosity, including chemical composition from the Alpha Particle X-ray Spectrometer, mineralogy from the CheMin instrument, and evolved gas and isotopic analyses from the Sample Analysis at Mars instrument, we show that the tridymite-bearing rocks exhibit similar chemical patterns with silica-rich alteration halos which crosscut the stratigraphy. We infer that the tridymite formed in-place through hydrothermal processes and show additional chemical and mineralogical results from Gale crater consistent with hydrothermal activity occurring after sediment deposition and lithification.

Plain Language Summary In August 2015, the Curiosity Mars rover discovered tridymite, an unexpected mineral phase, in Gale crater. The existing model for its occurrence suggests erosion and deposition from silicon-rich volcanic rocks in the crater rim or central peak. The chemistry and mineralogy of the tridymite-bearing rocks, however, are not consistent with silicon-rich volcanic material. Using data from Curiosity's instrument suite, we show that the tridymite-bearing rocks exhibit similar chemical patterns with silicon-rich alteration zones which crosscut the layered sediments. We infer that the tridymite formed in-place through hydrothermal processes and show additional chemical and mineralogical results from Gale crater consistent with hydrothermal activity occurring after sediment deposition and lithification.

1. Introduction

Understanding the past and present habitability of the martian environment is the focus of the Curiosity Mars rover investigation. Since landing in Gale crater in August 2012, the instrument payload has provided evidence for an ancient lacustrine system with extensive deposits of finely layered mudstone (Murray formation) (Grotzinger et al., 2015). The Murray formation includes a localized occurrence of high-silica rocks with tridymite ("Buckskin" sample) previously interpreted as a detrital accumulation of silicic volcanic material (Morris et al., 2016). The sedimentary rocks of the Murray formation are overlain by a younger aeolian sandstone (Stimson formation) (Banham et al., 2018) that has been locally altered to form narrow, silica-rich alteration halos (Frydenvang et al., 2017; Yen et al., 2017).

A new analysis of the available data suggests a strong chemical relationship between high-silica regions in the Murray and in the Stimson formations. The high-silica, fracture-associated alteration halos in the Stimson sandstone crosscut the bedding, indicative of post-depositional modification. We propose here that the tridymitic material in the Murray formation formed through similar processes. Specifically, as an alternative to a detrital origin, we advance the model that tridymitic material resulted from in situ hydrothermal silicification. We also show that many other aspects of the Curiosity data set are consistent with a hydrothermal history within Gale crater.

1.1. Methods

Chemical, mineralogical, and imaging data from the Curiosity rover through sol 2300 of martian surface operations were utilized for this study. The Alpha Particle X-ray Spectrometer (APXS; Gellert & Yen, 2019) establishes the bulk chemical composition of the material within its ~2 cm diameter field of view. The APXS utilizes radioactive curium sources to induce X-ray emissions that are measured with a silicon drift detector. Typically, 16 elements are quantified for each sample and ~10 additional trace elements can be quantified depending on abundances (Gellert & Yen, 2019). The rover's robotic arm can place the APXS sensor head on a variety of soil and rock targets including ones which have been modified by brushing (removal of dust) or drilling (drill tailings and sieved/dumped material).

The CheMin X-ray powder diffraction (XRD) instrument in the analytical laboratory portion of the Curiosity rover accepts drill samples delivered by the robotic arm through an inlet funnel at the top of the rover. The grains drop into reusable sample cells which are piezoelectrically actuated to randomize sample orientation while diffracted cobalt X-rays are measured in transmission by an area detector (Blake et al., 2012). X-ray diffraction patterns are processed and fit (e.g., Rampe et al., 2020) for quantitative abundances with commercial Rietveld refinement software as well as using the FULLPAT method (Chipera & Bish, 2002) for partially ordered and amorphous phases. The detection limit for mineral phases depends on degree of crystallinity and the extent of peak interferences but is typically ~1 wt%.

The Sample Analysis at Mars (SAM) analytical laboratory consists of three separate instruments: Quadrupole mass spectrometer, gas chromatograph, and tunable laser spectrometer (Mahaffy et al., 2012). Samples delivered to SAM for evolved gas analyses (EGA) are heated in a quartz cup to ~870°C with a helium carrier gas and analyzed by the mass spectrometer (Sutter et al., 2017). SAM is capable of a wide variety of other measurements including hydrocarbon detection with and without derivatization, isotopic composition of H_2O and CO_2, and atmospheric analyses (Mahaffy et al., 2012), but here we focus on the EGA.

The payload complement of the Curiosity rover also includes the ChemCam Laser Induced Breakdown Spectrometer (LIBS) for chemical composition of rocks and soils (Wiens et al., 2012), multispectral imaging with the Mast Camera (Mastcam) system (Bell et al., 2017), and the Mars Hand Lens Imager (MAHLI) for close-up imaging at scales as fine as ~14 microns/pixel (Edgett et al., 2012).

1.2. Problem Statement

The occurrence of tridymite, a low-pressure, high-temperature SiO_2 polymorph identified by CheMin in the Pahrump Hills member (Figures S1 and S2) of the Murray formation was previously attributed to detrital accumulations of silicic volcanic material (Morris et al., 2016). When that study was published, a detrital input was deemed the best option amidst alternatives such as high-temperature hydrothermal alteration, pyroclastic flows, and impact processes. Several aspects of this interpretation, however, remain puzzling. First, the relatively large amount of tridymite, ~34 wt% of the crystalline fraction and ~14 wt% in the bulk sample (Morris et al., 2016), requires deposition of tridymitic volcanic sediment which does not contribute material to any other sampled layer of the Murray formation. Second, with only ~6 wt% Al_2O_3, the Buckskin sample is not consistent with an unaltered evolved silicic igneous origin. The amount of bulk Al_2O_3, for example, in the rhyolitic Bandelier Tuff (New Mexico, USA) ranges between 11 and 15 wt% (Crowe et al., 1978). Third, the Buckskin TiO_2 content (1.7 wt%) is the highest measured through sol 2300 by the Curiosity rover and is not consistent with the lower TiO_2 abundances (<0.5 wt%) of typical terrestrial rhyolites. The SiO_2/TiO_2 ratio remains roughly constant across all Murray formation samples (Gellert & Yen, 2019) (average ratio = 45.8, standard deviation = 6.0, n = 495), including those with elevated silica (45.3 average, 1σ = 3.2,

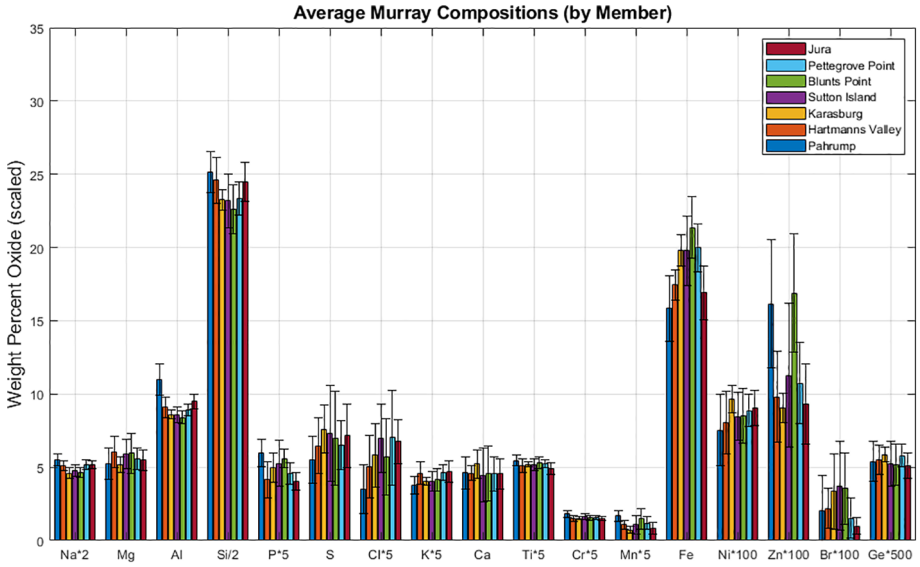

Figure 1. Average composition of members of the Murray formation (excluding veins and other calcium sulphate-rich samples; several elements scaled) illustrating relatively little chemical variation over 320 m of elevation. Stratigraphy of Murray formation shown in Figure S2. Error bars represent standard deviation of the measurements.

$n = 10$; range for Buckskin: 42.2 to 46.9) and would require an unlikely proportional influx of higher density TiO_2 minerals corresponding to the amount of lower density detrital tridymite to explain this observation. Fourth, the plagioclase composition of Buckskin (~An 40), which is consistent with other Murray samples (Morrison et al., 2018) is too calcic for terrestrial silicic volcanic rocks. If, however, the plagioclase is from a source typical of other Murray samples, then the absence of pyroxenes in the Buckskin sample (Morris et al., 2016) requires a removal process. Finally, cristobalite, another high-temperature, low-pressure silica polymorph is found in both Buckskin (2.4 wt%, Morris et al., 2016) and the nearby Telegraph Peak sample (7.3 wt%, Rampe et al., 2017) of the Murray formation. If this cristobalite were also a detrital component, it would require a separate source region for tridymite-free cristobalite.

In this study, we present an alternative hypothesis to the detrital origin of the tridymite and suggest that in situ formation of the silica-rich material under hydrothermal conditions would alleviate the chemical and mineralogical inconsistencies listed above.

2. Key Observations

2.1. Murray Formation

Through sol 2300, the APXS has analyzed over 700 Murray formation samples along its ~20 km traverse and nearly 400 m of elevation gain (Figures S1 and S2). With the exception of ~10 silica-enriched samples at and near the Buckskin drill location and those with a substantial calcium-sulphate component (>15 wt% SO_3 with correspondingly elevated CaO) or clear diagenetic features, their chemical compositions are remarkably uniform (Figure 1). Ti and Cr values, for example, vary from the mean by only 8% and 13% (relative, 1-sigma), respectively, which is roughly twice the precision of the measurement. Volatile elements such as Cl, Zn, Br exhibit the greatest variability, consistent with their geochemical mobility. P and Mn sometimes vary dramatically over short distance scales, and differences in their abundances across the members of the Murray formation (Figure 1) may reflect a history of fluid transport. Rocks of the Murray formation stratigraphically below the Buckskin sample (Pahrump) and in the 300 m of vertical section above the silica-enriched bedrock (Hartmann's Valley through Jura, Figure S2) have a consistent average chemical composition (Figure 1), suggesting that the sediments are dominated by a common source (as predicted by Kite et al. [2013b]). The compositional anomaly at the Buckskin location is therefore difficult to explain by irregularities in the detrital input and suggestive of post-depositional modification. Note that accumulations from direct fallout of volcanic ash for the silica-rich material in the Murray formation were

specifically excluded by Morris et al. (2016) due to the fine laminations of nearby silica-rich deposits, and further, airfall ash would not resolve the chemical (low Al_2O_3, high TiO_2) and mineralogical (plagioclase composition) issues described in Section 1.2.

2.2. Alteration Relationships

Occurrences of high-silica bedrock analyzed by APXS at Gale crater include: (1) ~50-cm wide alteration halos in the Stimson sandstone (Figures 2a and 2b) (Yen et al., 2017), (2) a similar-sized alteration halo in the Murray mudstone (Yen et al., 2017), and (3) tridymitic bedrock exposed at the Buckskin drill location in the Murray formation immediately below Stimson formation rocks (Morris et al., 2016; Figure 2c). The first two examples reflect alteration in narrow zones crosscutting the stratigraphy while the third is of greater areal extent with no observed margins of the silicified material, but all three exhibit nearly identical patterns of depleted (Mg, Al, Mn, Fe, Ni, Zn) and enriched (Si, S, P) elements relative to nearby rocks (Figures 3 and S3). *Thus, the chemical composition of the high-silica, tridymitic bedrock can be produced through alteration of typical Murray formation material analogous to the development of the nearby alteration halos*. The formation process for the alteration halos likely involves acid-sulphate alteration and silicification of the parent rock (Hausrath et al., 2018; Yen et al., 2017), and the chemical similarities indicate that the tridymite-bearing region likely interacted with the same fluids.

The EGA (Figure 4) from the SAM instrument (Mahaffy et al., 2012) provide further evidence for the connection between the tridymite-bearing Murray and the alteration halos. The sample acquired from the Stimson alteration halo (Greenhorn) exhibits a SO_2 release at ~875°C which is largely absent from the parent Stimson sample (Big Sky) (Sutter et al., 2017). This high-temperature SO_2 release, which is consistent with the presence of $MgSO_4$, is also found in the elevated-silica Buckskin sample but is different from the SO_2 release profile in other Murray drill samples (Sutter et al., 2017). Indication of similar sulfur-bearing fluids infiltrating both silicified Murray and Stimson alteration halos is supported by the uniquely enriched sulfur isotopes of the evolved gases: The ^{34}S released from the silicified samples is enriched in all temperature ranges, which is distinct from the parent Stimson material outside of the alteration halos and from other Murray formation samples (Franz et al., 2017). Oxygen isotopes also connect the Buckskin sample to the Stimson (Franz et al., 2020).

In addition to the chemical, evolved gas, and isotopic similarities from the APXS and SAM instruments, ChemCam data connect unique hydration signatures (presence of opal-A) in the alteration halos and the high-silica Murray samples consistent with related diagenetic origins (Rapin et al., 2018). Further, the chemical composition of the large amount (50%–75%) of amorphous material in the silica-rich drill samples (calculated by subtracting CheMin-derived crystalline chemistry from the APXS composition of the drill fines) are characteristically depleted in aluminum (Morris et al., 2016; Yen et al., 2017) suggestive of mobility in acidic fluids. Note that the ChemCam instrument established that an alteration halo (target name "Kukri", Figure 2g) encountered early in the mission (sol 392) in the Bradbury formation (Figure S2), exhibited similar chemical characteristics to the alteration halos found in the Stimson formation (Bedford et al., 2019; Williams et al., 2014). This sample, however, was not analyzed by APXS nor the analytical laboratory instruments.

3. Discussion

In light of the issues (Section 1.2) with the model of detrital accumulation of silicic volcanic material from the crater rim or central peak (Morris et al., 2016), and given the recent understanding that the chemical composition of the tridymite-bearing sample can be derived through alteration of typical Murray rocks in a manner similar to the alteration halos (Figure 3) as well as similarities in the evolved gas analysis results (Figure 4), we propose here that the tridymite formed in place.

Other work has described relationships between the high-silica Murray rocks and the alteration halos cross-cutting the Stimson formation, but these models are quite different. Frydenvang et al. (2017) support detrital silica-emplacement in the Murray formation and suggest that neutral to alkaline pH fluids carried silica through fractures into the overlying Stimson formation where it precipitated. This model, however, does not address the chemical and mineralogical issues described in Section 1.2, and geochemical mass

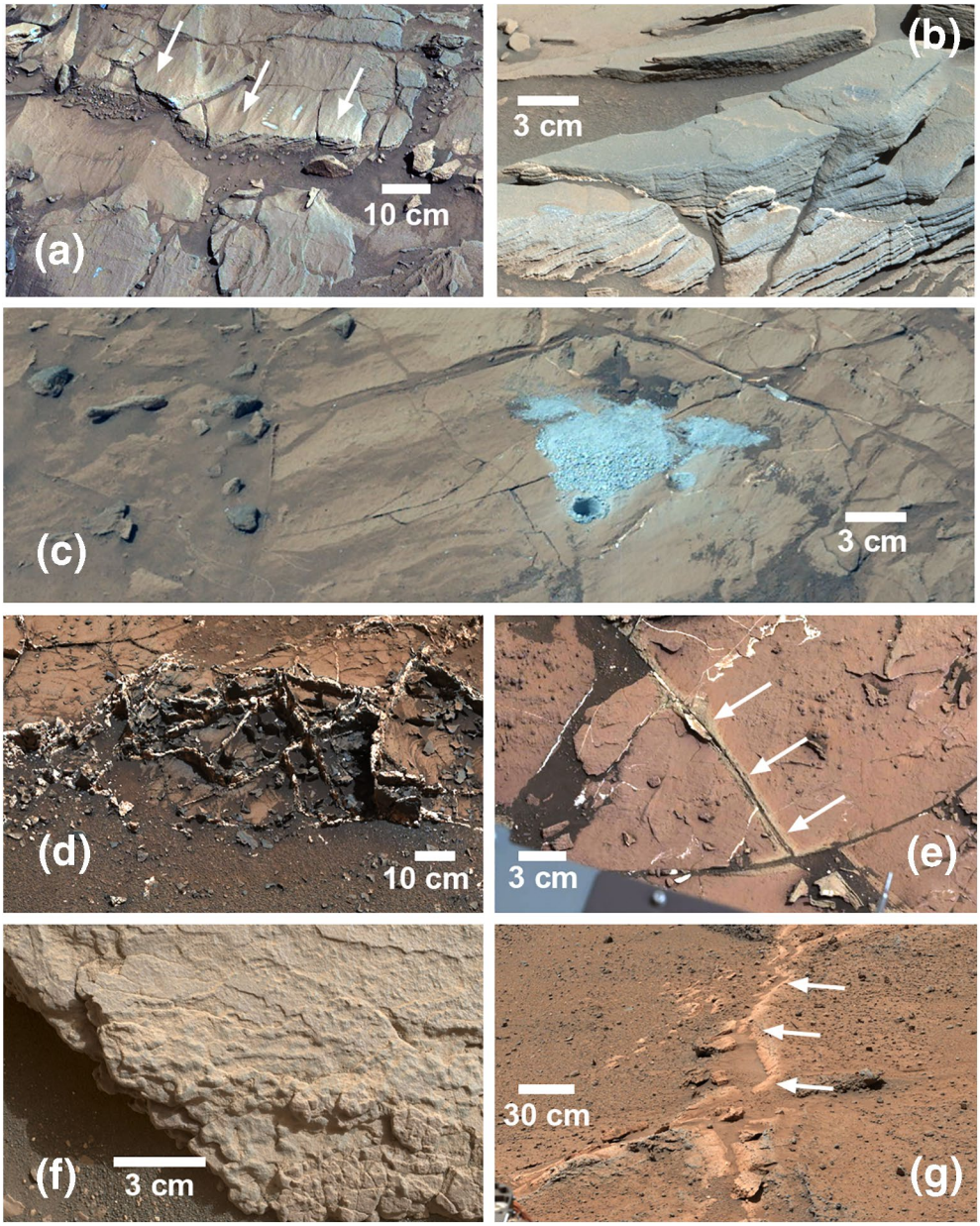

Figure 2. (a) Alteration halo in Stimson sandstone (Lubango target, portion of mcam06284, sol 1317), (b) silicified, layered Stimson sandstone (lighter left half, 67 wt% SiO_2; darker right half 42 wt% SiO_2) showing that primary textures can survive the silicification process (portion of mcam06267, sol 1314), (c) tridymite-bearing Buckskin drill hole (portion of 1060ML0046620010104720E01, sol 1060), (d) Garden City vein complex (portion of mcam04073, sol 926), (e) K- and Se-enriched small alteration halo (Thrumcap, portion of mcam07625, sol 1503), (f) Se-rich nodular rock (Berry Cove, MAHLI sol 1714), (g) alteration halo encountered early in mission ("Kukri," mcam01617, sol 392, (Williams et al., 2014; Bedford et al., 2019)).

balance and reactive transport modeling indicate interactions with acidic fluids in the formation of the alteration halos (Hausrath et al., 2018). Czarnecki et al. (2020) proposed that the silica-rich material found at Buckskin is part of a stratigraphically conformably layer >17 km in lateral dimension derived from the erosion of volcanic rocks in the Gale lake catchment. Detrital silicic volcanics do not address the chemical and mineralogical issues listed in Section 1.2, and further, given the large volume of source material required to produce such an expansive deposit, it seems unlikely that erosional deposition could be limited to a single drilled sample in the Murray formation.

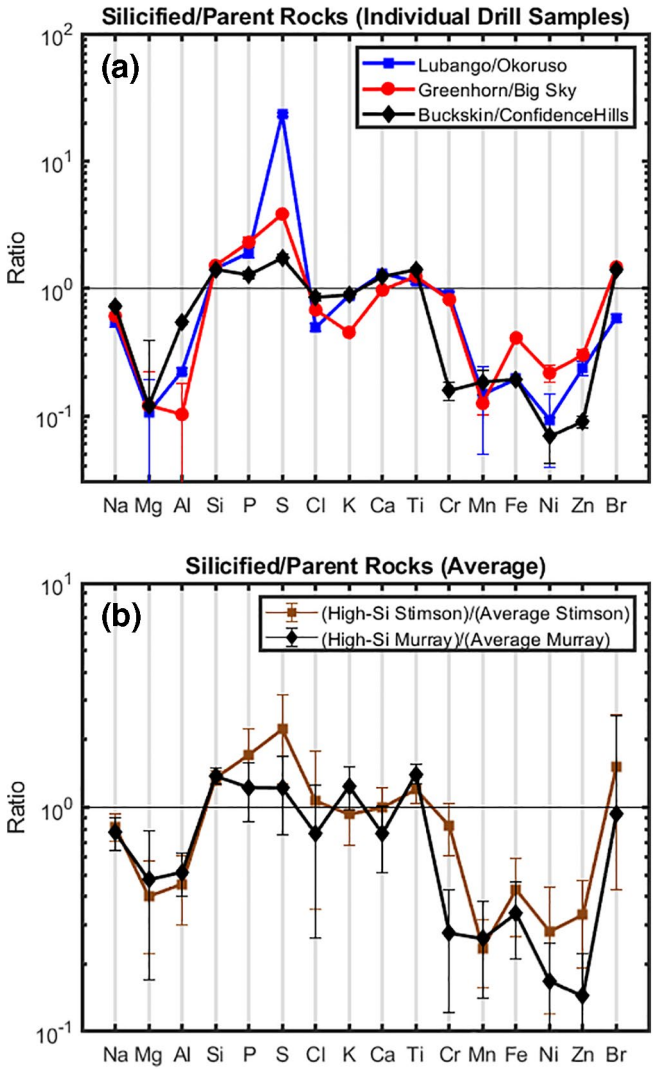

Figure 3. Chemical composition ratios for silicified samples. (a) Drill samples from the Stimson formation (Lubango and Greenhorn) relative to parent material (Okoruso and Big Sky, respectively) and from the Murray formation (tridymite-bearing Buckskin sample relative to the drill hole at Confidence Hills). The chemical composition of each drill hole is represented by Alpha Particle X-ray Spectrometer (APXS) analyses of unsieved drill hole cuttings. (b) Average for all elevated-silica Stimson samples relative to typical (nonsilicified) compositions and average of all elevated-silica Murray samples relative to the average composition of the nearby Pahrump Hills member of the Murray formation. Similar patterns of enrichment and depletion indicate that the fluids responsible for the alteration halos in the Stimson sandstone could have produced the chemical composition of the tridymite-bearing Buckskin target.

3.1. Tridymite Formation

The thermodynamic stability field for tridymite at low pressure is between 870°C and 1,470°C, but it exists metastably at lower temperatures. Above ~380°C, the crystal structure of tridymite is dominantly hexagonal with minor distortion of the Si-O-Si bond angles and Si-O bond length (Kihara et al., 1986). Between 380°C and 110°C, tridymite transitions to various orthorhombic forms, and below 110°C, monoclinic tridymite is prevalent (Heaney et al., 1994). Monoclinic tridymite with sharp, well-defined XRD peaks (FWHM = 0.27°) is the form detected in the Buckskin drill sample on Mars (Morris et al., 2016).

The Buckskin tridymite could have evolved from basaltic progenitors through in situ silicification and exposure to temperatures within its thermodynamic stability field (>870°C). Tridymite has been reported in terrestrial fumarolic environments where vapors induce dissolution and reprecipitation of wall rock producing secondary phases such as sulfates, iron oxides, tridymite, cristobalite, and various other silicates occurring in layered, filled cavities or as veins in the host rock (Ganino et al., 2019; Getahun et al., 1996). Fumarolic deposits in Kamchatka exhibit secondary mineral assemblages composed of anhydrite, Al and Fe sulfates, Ti oxide, cristobalite, tridymite, quartz and pyrite or hematite (Ganino et al., 2019). Low pH fumaroles in basaltic andesites in Nicaragua contain sulfur, gypsum, amorphous silica, cristobalite, tridymite, hematite, and phyllosilicates (Hynek et al., 2013). In Japan, high-temperature, acid-sulphate solutions and vapors chemically leached the parent rock leaving a residue of SiO_2, TiO_2, and P_2O_5 while increasing the tridymite abundance (Hamasaki, 2002), and in the Philippines, acid derived from native sulfur completely leached the country rock to opal, cristobalite, and tridymite (Reyes, 1990). These tridymite-containing mineral assemblages presumed to have formed at high-temperatures (>870°C) are consistent with the phases found at the Buckskin drill site: Plagioclase feldspar (parent rock), sanidine, magnetite, anhydrite, cristobalite, opal-CT and other X-ray amorphous phases.

In contrast to high-temperature formation scenarios, tridymite has been predicted to occur below its thermodynamic stability limit of 870°C when rapid growth rates are present (Jones & Segnit, 1972). Fumarolic and hydrothermal mineral assemblages containing tridymite have been collected at 640°C (Getahun et al., 1996) and between 300°C and 500°C (Ganino et al., 2019), but the possibility that temperatures were higher (within the stability field of tridymite) at the time of formation is not precluded. Other papers describing the natural occurrence of tridymite suspected to have formed at lower temperatures (e.g. Klasik et al., 1975; Ostrooumov, 2007) generally do not provide sufficient data to rule out the possibility that the observations involve opal-CT. The atomic structure of opal-CT is not well understood (Curtis et al., 2019; Ghisoli et al., 2010) and has been variably interpreted as disordered stacking of cristobalite (C) and tridymite (T) units (e.g., Guthrie et al., 1995) or amorphous opaline silica with crystalline domains of a dominantly tridymitic nature (Wilson, 2014). The degree of order and volume fraction of cristobalite and tridymite in opal-CT affects the XRD pattern, where samples can exhibit peaks at lattice d-spacings of 4.31 Å, 4.10 Å, and 3.91 Å (opal-CT from cavity of hydrothermal geode) (Ilieva et al., 2007) and at 4.27 Å, 4.08 Å, and 3.89 Å (opal-CT from an iron mine in Australia) (Curtis et al., 2019). The peak locations of the tridymite discovered in the Buckskin sample on Mars (4.31–4.32 Å, 4.10 Å, 3.81–3.83 Å) (Morris et al., 2016) are roughly comparable, though the peak widths are much more narrow in the martian sample.

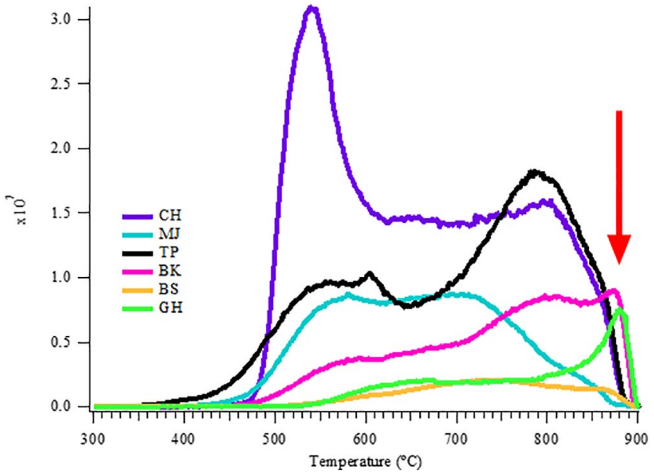

Figure 4. Sample Analysis at Mars (SAM) evolved gas analyses (EGA) SO_2 release profiles in counts/second showing that the high temperature release (arrow) found in the silica-rich, tridymite-bearing Murray formation (BK-Buckskin) and the silica-rich alteration halo in the Stimson formation (GH-Greenhorn) is not found in any of the Murray formation samples closest to Buckskin in the Pahrump Hills member (CH-Confidence Hills, MJ-Mojave2, TP-Telegraph Peak) nor in the parent, nonsilicified Stimson sample (BS-BigSky). This is an indication that unique sulfur-bearing fluids were associated with the silicified samples.

The existence of a tridymite-like endmember to the opal-C to opal-CT series has been hypothesized, and although tridymite domains are clearly common in opals, the identification of a true opal-T endmember remains elusive (Elzea & Rice, 1996). Examples of opaline silica dominated by tridymite structures include deposits in a marine environment resulting from interactions with hot Si-rich solutions (Ilieva et al., 2007) and precipitates from hydrothermal solutions in vugs of altered silicic volcanic rocks (Tada & Iijima, 1982). Diagenetic microcrystalline opal-CT was found to contain tabular platelets of tridymite ~100 nm in size (Cady et al., 1996). While volumetrically minor, these tridymite domains exhibit optical diffractograms from high-resolution transmission electron microscopy consistent with well-ordered material (Cady et al., 1996). Furthermore, a low-temperature, hydrothermally precipitated assemblage of cristobalite, opal-CT, and tridymite was shown to contain tridymite domains greater than 1 micron in scale, which exhibit well-crystalline electron diffraction and sharp synchrotron XRD patterns (Lee & Xu, 2019). Collectively, these results indicate that the precipitation of silica under hydrothermal conditions at temperatures less than 870°C can produce micron-scale crystalline tridymite domains in association with opal-CT.

The atomic structure of silica precipitated from hydrothermal fluids likely depends on factors such as fluid chemistry (including degree of silica supersaturation), time, temperature, and nature of nucleation sites. Given the incomplete understanding of opal-CT structures, some of which contain crystals of ordered tridymite, the possibility that the unique martian environment resulted in the development of significant monoclinic tridymite in hydrothermal conditions at temperatures less than 870°C should be considered. In fact, the Buckskin sample was modeled to contain opal-CT (6 wt%) and cristobalite (2.4 ± 0.3 wt%) in addition to monoclinic tridymite (13.6 ± 0.8 wt %) (Morris et al., 2016). With strong chemical evidence that the silicified material at Buckskin formed in place and the difficulties with the detrital tridymite interpretation, we suggest that the hydrothermal precipitation of opaline silica with crystalline cristobalite and tridymite domains large enough to produce sharp XRD lines be considered as a candidate explanation for the observations.

3.2. Chemical Evidence Supporting Hydrothermal Activity

A number of additional chemical characteristics established by the APXS of the rocks in Gale crater are consistent with in situ hydrothermal alteration. For example, the P_2O_5 concentrations in the alteration halos (1.5 ± 0.4 wt%) and the Buckskin region (1.5 ± 0.4 wt%) are the same and notably higher than unaltered Stimson (0.8 ± 0.1 wt%) and Murray formation (1.0 ± 0.2 wt%) rocks. Retention of P_2O_5 is an observed characteristic of terrestrial hydrothermal, acid-sulphate alteration and P_2O_5 is one of the few oxides (in addition to TiO_2 and SiO_2) which is resistant to leaching under these conditions (Hamasaki, 2002), possibly resulting from dissolution and local reprecipitation as insoluble phosphates (Dill, 2001).

On the basis of the relatively high concentrations of Zn (~1,000 ppm) and Ge (~100 ppm) across diverse sedimentary lithologies, Berger et al. (2017) argued that hydrothermal fluids concentrated these elements in the source region prior to accumulation in the crater and subsequent diagenetic fractionation. Here, we suggest that in addition to possible hydrothermal enrichments from the source region, vapor phase and associated hydrothermal activity occurred after the deposition and lithification of the Murray sediments. One of the highest concentrations of Ge measured at the surface of Mars (~650 ppm) is found in the Garden City vein complex (Berger et al., 2017), a network of dominantly calcium-sulphate veins cross-cutting Murray bedrock (Figure 2d). This 7-fold enrichment over surrounding rocks has been attributed to Ge mobility in F-bearing diagenetic fluids (Berger et al., 2017), given detections of fluorine by the ChemCam instrument (Nachon et al., 2017). The solubility of Ge, however, increases with temperature, and hydrothermal fluids are also capable of mobilizing and concentrating Ge (Pokrovski & Schott, 1998). Consistent with a hydrothermal association, the APXS analyses show large concentrations of Cu (~150 ppm), an element with

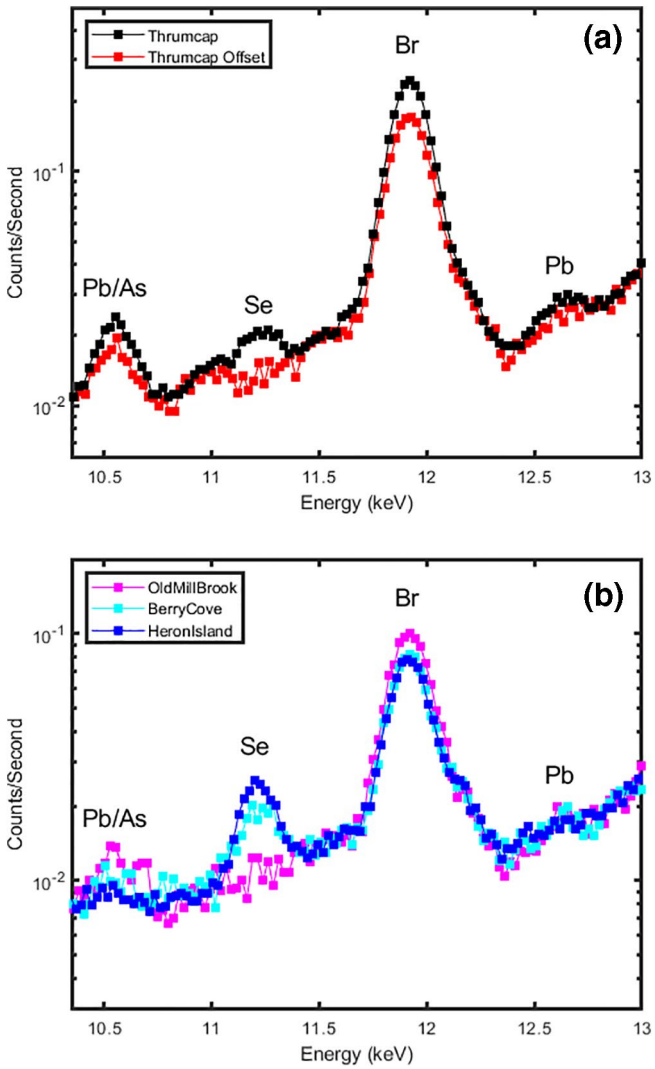

Figure 5. (a) Selenium enrichment in Thrumcap alteration zone (Figure 2e) relative to bulk rock. (b) Selenium enrichment in nodular, gray Murray samples, Heron Island (Figure 2f) and Berry Cove, relative to typical Murray mudstone (Old Mill Brook).

increased solubility at elevated temperatures (Liu & McPhail, 2005), in the dark portions of the veins. These levels of Cu are among the highest measured at Gale crater and are ~3 times the average Murray host rock concentration. Notably however, the Ge in the tridymite-bearing region is depleted (~50%) relative to the unaltered rocks, and Cu is at/near the detection limit. The mobility of Ge (and likely Cu) is consistent with hydrothermal systems where Ge is scavenged from the host rock (Arnorsson, 1984) and precipitated elsewhere as the fluids cooled or evaporated.

Further suggestions of fluid mobility at elevated temperatures in the Murray formation are preserved in the centimeter-scale alteration halo of the target Thrumcap (Figure 2e). Relative to the surrounding host rock, the lighter-toned central region shows roughly double the amounts of K_2O and SO_3, indicative of elements transported in the fluid. Importantly, the altered zone contains at least five times the selenium of the surrounding rock (Figure 5). Additionally, Se is typically enhanced in gray, nodular features relative to surrounding Murray formation rocks (Figure 2f). These samples may represent incipient diagenetic concretions and reflect the mobility of Se in fluids. The majority of terrestrial selenium deposits are associated with hydrothermal processes (Stillings, 2017), and elevated concentrations are used as indicators of high temperature (~350°C) interactions (Auclair et al., 1987; Wang et al., 2017). While selenium can also accumulate in sedimentary basins because of weathering (Stillings, 2017), the lateral heterogeneity across the Thrumcap alteration halo and in nodular features indicates its introduction through fluid mobility. The occurrence of elevated Se in these Murray formation rocks is consistent with hydrothermal activity; however, this interpretation is not unique, as low pH fluids (Krivovichev et al., 2017) could also be responsible for its mobility.

Lead, another element which is highly mobile in hydrothermal fluids (Fishman & Hem, 1976), is found in varying amounts in the Murray formation by the APXS with some samples exceeding 200 ppm. Correlations with Se in localized regions (Figure S4) support the possibility that both elements could have been mobilized in hydrothermal fluids. Ni and Zn concentrations are also elevated and laterally variable in Murray formation samples relative to basaltic rocks and soils. While the mobility and concentration of these trace elements are not uniquely associated with mobility in hydrothermal systems, their occurrences are consistent with interactions with fluids at elevated temperatures.

3.3. Mineralogical and Isotopic Evidence Supporting Hydrothermal Activity

Further evidence for hydrothermal fluid mobility is supported by the mineralogical data set established by the CheMin instrument in conjunction with APXS and SAM instrument results. Analyses have identified mineral phases in addition to tridymite which may be consistent with hydrothermal activity within Gale crater over a wide range of temperatures. Ferripyrophyllite, for example, is a high-temperature (200°C–320°C) hydrothermal alteration product (Reyes, 1990) which has been identified in the Murray formation. The first detection of ferripyrophyllite at the Oudam drill site (Figures S1 and S2) was attributed to a detrital component, given the relatively low abundance (Bristow et al., 2018). However, isotopic data from sulfides within this sample are consistent with fractionation at elevated temperatures (Franz et al., 2017). With multiple recent detections of ferripyrophyllite on the Vera Rubin Ridge (Figure S1), direct precipitation from warm, acidic fluids or alteration of pre-existing phyllosilicates has been proposed (Rampe et al, 2020).

Other phyllosilicates identified by the CheMin XRD in Murray formation drill samples include dioctahedral smectite or illite (Rampe et al., 2017) and trioctahedral smectite such as saponite (Bristow et al., 2018; Vaniman et al., 2014). The identification of the phyllosilicates is based on diffraction peaks from the basal (001) spacing and the clay mineral band (02l) and augmented by APXS chemistry and SAM EGA data (e.g., Bristow et al., 2018; Rampe et al., 2020). The amount of phyllosilicate present generally ranges between 10 and 30 wt%. Each phyllosilicate has multiple pathways for formation and emplacement, including exposure to fluids at elevated temperatures. Saponite found in nakhlites, for example, is a hydrothermal alteration product (Hicks et al., 2014), though the context is different (found in fractures in nakhlites vs. bulk saponite in sedimentary rocks at Gale crater). Some pathways to minerals more definitive for hydrothermal alteration (e.g., chlorite, serpentine, talc) progress through smectites and other phyllosilicates (Beaufort et al., 2015) detected by CheMin. While syn-depositional, aqueous alteration of basaltic material in a near-surface environment has been hypothesized for the formation of most clay minerals at Gale crater (Bristow et al., 2018), hydrothermal pathways are also possible.

Nonphyllosilicate phases identified by CheMin may also have hydrothermal origins. Anhydrite, for example, is abundant in drill samples and likely precipitated directly from solution instead of from gypsum dehydration (Vaniman et al., 2018). Low water activity or elevated temperatures both support the direct formation of anhydrite, but given associations with soluble salts, precipitation from saline solutions at temperatures below ~50°C was suggested by Vaniman et al. (2018). Formation of anhydrite at higher temperatures and in fumarolic deposits, however, is common (Hannington et al., 2001; Zimbelman et al., 2005) and cannot be excluded. One scenario for the occurrence of calcium sulfates in multiple hydration states at Gale crater involves the initial formation of anhydrite at low water activity or high temperatures, the hydration to gypsum for samples exposed to low-temperature fluids, and subsequent dehydration from gypsum to bassanite (Rapin et al., 2016).

Sanidine derived from hydrothermal alteration of plagioclase-bearing tephra has been observed on Maunakea, and by analogy, sanidine occurrences (up to 5 wt%) in Murray formation samples are interpreted as possible hydrothermal alteration products of martian basaltic materials (Morris et al., 2020). This interpretation is consistent with the evidence for the fluid mobility of potassium discussed in Section 3.2. The Al-Si disorder observed in the martian sanidine samples is consistent with rapid precipitation at ~250°C (Morris et al., 2020). Furthermore, hematite and magnetite, which can also be associated with hydrothermal deposits, are abundant in the Gale crater sediments (up to 16 wt% hematite, and 8 wt% magnetite) (Bristow et al., 2018; Rampe et al., 2017, 2020). Detections of gray hematite from recent samples along the Vera Rubin Ridge are consistent with hydrothermal alteration at 100°C–200°C (Morris et al., 2020; Rampe et al., 2020).

Cristobalite was identified in the tridymite-bearing Buckskin sample as well as in the nearby Telegraph Peak drill hole (which did not contain tridymite). These two targets were among the few drill samples that were also modeled to contain opal-CT. If the cristobalite were detrital accumulations of this high-temperature (>1,470°C) SiO_2 polymorph, it would seem an unlikely coincidence that the only two samples through sol 2300 that contain cristobalite are also among the few that also contain opal-CT. More likely, these components are related. Cristobalite is difficult to discern from well-ordered opal-C by XRD (Elzea et al., 1994; Hillier & Lumsdon, 2008), suggesting that what has been identified as "cristobalite" could very well be opal-C, which forms in close association with opal-CT and can be found in low-temperature hydrothermal systems (Komatsu et al., 2019).

These variations in mineralogy in the Murray formation, not including the Buckskin sample, (e.g., 0–28 wt% phyllosilicates, 1–16 wt% hematite, 0–8 wt% magnetite, 0–5 wt% sanidine by bulk) are from a sequence of sedimentary rocks which are nearly uniform in average chemical composition (Figure 1). For example, one drill sample (Stoer, 14.7 wt% hematite) (Rampe et al., 2020) has more than double the amount of hematite of a nearby sample (Duluth, 6.1 wt% hematite) (Rampe et al., 2020) but contains the same total iron (~22 wt%). Input from sediments with different compositions is possible, but in situ alteration without extensive leaching may be a better explanation for the differences in mineralogy with only minor difference in chemistry.

Further support for a hydrothermal history at Gale crater is evident in the sulfur isotopic signatures in certain drill samples. SO_2 is released at pyrolysis temperatures consistent with oxidation of Fe-sulfides during SAM analyses of the Oudam sample of the Murray formation and the Cumberland sample from the

lower-elevation Yellowknife Bay. These two samples are significantly depleted in ^{34}S, interpreted to indicate isotopic fractionation in a hydrothermal system (Franz et al., 2017) and contain phyllosilicates suggestive of hydrothermal alteration. Ferripyrophyllite discovered at Oudam from an observed 9.6 Å basal spacing (Bristow et al., 2018) is discussed above. CheMin results from Cumberland indicate a phyllosilicate with large interlayer spacing (13.2 Å) consistent with incipient chloritization resulting from exposure to a saline lake environment or to hydrothermal fluids (Vaniman et al., 2014). The observation of ^{34}S depletions only at isolated sites, such as at Cumberland but not the John Klein drill site a few meters away, suggests that the associated hydrothermal network produced highly localized alteration of the sediments (Franz et al., 2017).

Individually, each observation listed in this section could have alternative explanations. Collectively, however, and given the issues identified with the current interpretation for the origin of the tridymite, these observations support a history of hydrothermal alteration within Gale crater.

3.4. Heat Source

Thermal models accounting for a range of surface temperatures, burial depths, heat flow models, and thermal conductivity predict peak paleotemperatures along the Curiosity traverse between 80°C and 125°C for "baseline" scenarios (Borlina et al., 2015). Maximum modeled temperatures reach 225°C for assumptions involving a large sedimentary overburden, low thermal conductivity, and a high heat flow, though the authors suggest that temperatures above 150°C–225°C are not likely for burial alone without an additional source of heat such as hypervelocity impact or local volcanism (Borlina et al., 2015). Gravimetric data from Curiosity's accelerometers are consistent with shallow burial depths (<~1,800 m) (Lewis et al., 2019), which significantly limits the maximum predicted paleotemperatures (Borlina et al., 2015) in the absence of additional heat sources.

The hypervelocity impact that created Gale crater is modeled to have generated a melt pool between 0.5 and 1 km thick (Schwenzer et al., 2012) which would have taken several hundred thousand years to cool. Abramov and Kring (2005) estimated 380,000 years for a crater of 180 km diameter to cool to 90°C at 1 km below the surface, but higher temperatures would persist at greater depths which could continue to generate hydrothermal fluids. Most of the post-impact upwelling is modeled to occur in the peak ring region due to the impermeability of the high-temperature melt sheet below the central peak, and weak circulation of hydrothermal fluids could persist 2 Ma after the impact (Abramov & Kring, 2005). Recent studies of drill cores from the ~180 km diameter Chicxulub peak-ring crater (Yucatan Peninsula, Mexico) indicate post-impact temperatures of 300°C–400°C and that the hydrothermal system remained above ~100°C–250°C for 150,000 to 500,000 years (Kring et al., 2020). The Chesapeake Bay impact melt exceeded 1,700°C, and temperatures remained between 870°C and 1,000°C for a sufficient duration to produce tridymite and cristobalite (Jackson et al., 2011).

Volcanic activity is also a possible heat source for the formation of the tridymite and is likely required if the tridymite formed at temperatures above 870°C. Relatively recent volcanic activity on Mars is indicated by the occurrence of flood lavas associated with Elysium and Cerberus that may be less than 700 Ma, indicating that the upper mantle still had sufficient heat late in martian history to produce large volumes of low-viscosity melt (Plescia, 1990). While these flows only extend to ~500 km from Gale crater, and there is no clear surface expression of volcanic activity within the crater, a subsurface fracture system, perhaps associated with the dichotomy boundary or Gale impact fracturing may have provided conduits for hydrothermal fluids. The intrusive to extrusive magmatism ratio is modeled to be larger for Mars than for the Earth (Black & Manga, 2016), possibly contributing to the absence of volcanic features at the surface. The occurrence of relatively recent aqueous activity at Gale crater, perhaps thermally driven, is supported by K-Ar dating that indicates a fluid alteration event at 2.12 ± 0.36 Ga (Martin et al., 2017), and recent seismic detections by the InSight mission in Cerberus suggest that tectonic stresses and thermoelastic cooling continue into present day Mars (Giardini et al., 2020). Relatively young geologic activity may be consistent with the presence of a residual subsurface volcanic heat source after the deposition and lithification of sediments in Gale crater.

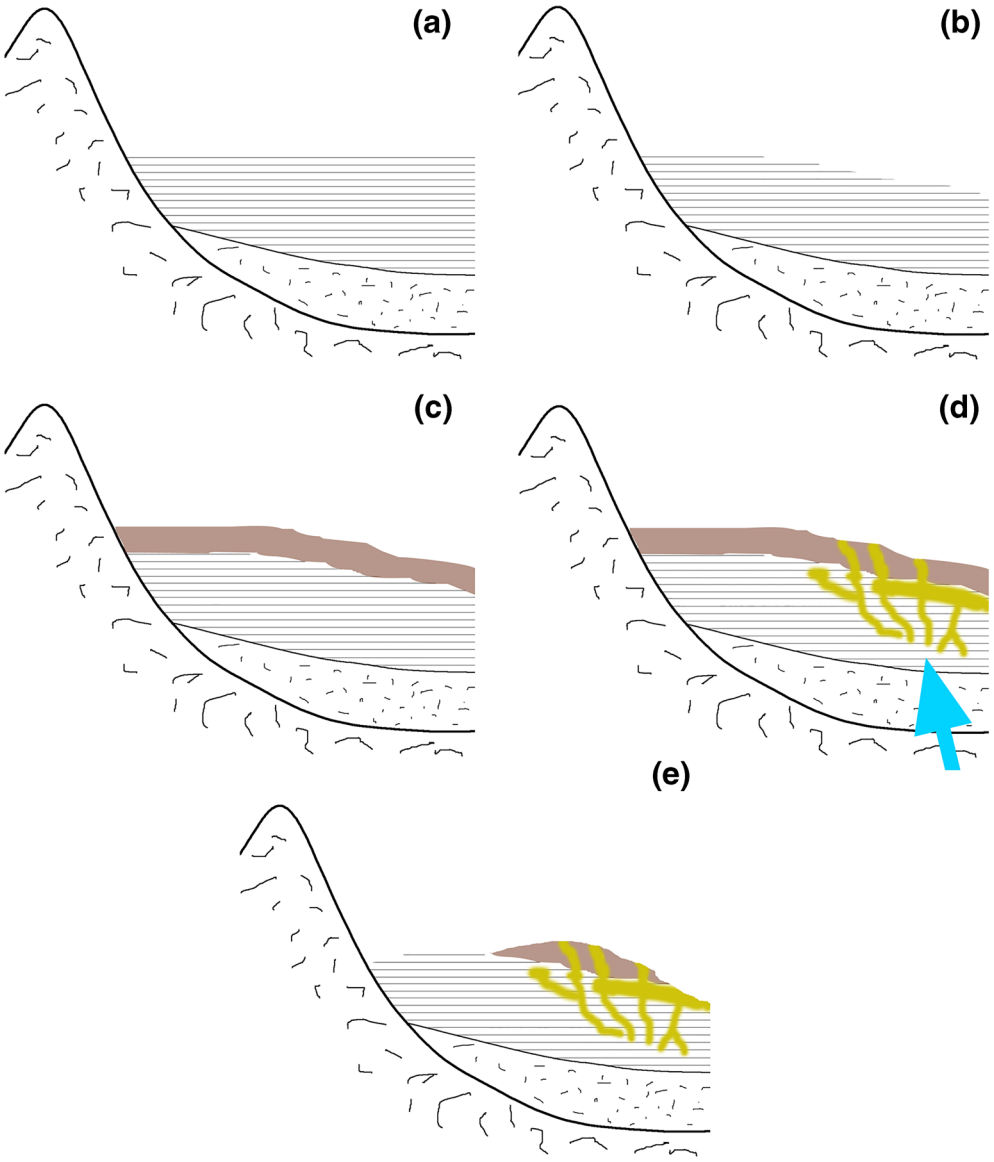

Figure 6. Conceptual scenario for the development of silica-rich material through hydrothermal activity at Gale crater: (a) Deposition and lithification of Murray formation sediments in Gale crater, (b) erosion of Murray formation, (c) deposition and lithification of Stimson formation sandstone, (d) hydrothermal alteration episode (influx of fluids depicted by blue arrow) creating alteration halos in the Stimson and Murray formation rocks and a silica-rich horizon in the Murray formation at the base of the Stimson, (e) further erosion exposing silica-rich Murray rocks.

3.5. Scenario

A hydrothermal system driven by residual heating from the Gale impact event could be responsible for the observed chemical and mineralogical signatures, especially if the sedimentation rates were high and the Murray and Stimson formations developed early in the history of the crater. A scenario for crystalline tridymite development from opal-CT at temperatures less than 870°C is described above, but if the tridymite formed within its stability field, the presence of a nearby volcanic heat source may be required. For either of these possibilities, the evolution of Gale crater could have proceeded as follows (Figure 6):

- The Gale impact event creates a subsurface network of fractures and future fluid conduits. Impact-associated hydrothermal processes may have altered rocks and soils in and around the impact basin (e.g., Schwenzer et al., 2012)

- Sedimentation of fines from a system of intermittent lakes over 10^4–10^7 years (Grotzinger et al., 2015) builds what we now find as the Murray formation. Alternatively, given the relative uniformity in chemical composition of the fines over 320 m of elevation (Figure 1), the development of the Murray formation may also be consistent with accretion thorough aeolian deposition (Kite et al., 2013a)
- Lithification and erosion of the Murray formation is followed by deposition and lithification of the overlying Stimson formation rocks
- Subsurface fluids in the Gale basin interact with impact-heated rocks or volcanic material resulting in the distribution of hydrothermal fluids and vapors through the fractures created by the impact event. These fluids migrate through the overlying Murray and Stimson formations producing the silica enrichment (including tridymite) and alteration phases observed by the Curiosity rover. Alteration occurs along fractures and in localized regions along the Murray-Stimson contact (Buckskin drill hole is less than ~20 cm below the Murray-Stimson contact)
- Compositional variability measured by the rover instruments over short distance scales is consistent with temperature gradients observed in terrestrial hydrothermal environments (Africano et al., 2003). The highest activity region may have been the tridymite-bearing locale of the Murray formation. Hydrothermal signatures are widespread within Gale crater with minerals consistent with a hydrothermal history in many Curiosity drill samples. Fluid conduits are observed at higher (Yen et al., 2017) and lower (Figure 2g) elevations relative to the tridymite, and many of these conduits are found in proximity to the Buckskin drill location
- Multiple generations of fluid transport at various temperatures may have produced additional overprints on earlier alteration phases, including mobility of trace elements (Section 3.2) and mineralization (Section 3.3)

3.6. Issues

This scenario of hydrothermal alteration within Gale crater is supported by many rover observations, but several possible inconsistencies remain. First, a small (10 cm), silicified (73 wt% SiO_2) rock (Figure S5) 10 m from the tridymite-bearing drill hole exhibits millimeter-scale primary laminations which seem too well preserved to have experienced high-temperature alteration. It is not known, however, if this rock contains tridymite, as it was not analyzed by CheMin. Silicified rocks at Gale crater can maintain pre-existing textures (Figure 2b), and large temperature gradients over short distance scales characteristic of hydrothermal systems may have resulted in a different thermal history for this rock allowing preservation of the layering. Furthermore, scanning electron microscope images of terrestrial hydrothermal deposits show close associations between primary igneous phases and secondary alteration and that replacement of primary phases allow retention of original textures (Ganino et al., 2019).

A second possible inconsistency is the absence of tridymite detections in silica-rich alteration halos found in the Stimson sandstone (Yen et al., 2017). However, given that the closest alteration halo analyzed by CheMin (Greenhorn) is 320 m laterally and 12 m vertically from the tridymite-bearing sample, localized, high temperature fluids and vapors associated with tridymite formation may have cooled over the distance and in the fractures leading to the sandstone locations sampled by Curiosity. The second alteration halo (Lubango) analyzed in detail is 900 m laterally and 19 m vertically from the tridymite-bearing sample.

Some have questioned whether the minerals detected at Buckskin are consistent with a high-temperature mineral assemblage. It is possible that definitive high-temperature phases are present below the ~1 wt% detection limit of the CheMin XRD for crystalline phases, but terrestrial hydrothermal deposits containing tridymite are primarily associated with sulfates and amorphous/crystalline silica (including cristobalite) (Ganino et al., 2019; Reyes, 1990). Alteration products can include magnetite and sanidine (Africano et al., 2003; Getahun et al., 1996). Thus, the crystalline mineral phases found in the Buckskin drill sample are in fact consistent with those found in some terrestrial high-temperature hydrothermal deposits: Tridymite, sanidine, magnetite, cristobalite, and anhydrite plus plagioclase (Morris et al., 2016) from the original host rock.

Finally, if the tridymite formed within its thermodynamic stability field (>870°C), heat transport from a putative subsurface volcanic source through the underlying rocks to the elevation of Buckskin (Figure S2)

could present a challenge. The largest observed fluid conduits may only be on the scale of centimeters, and conductive heat loss to the wall rock would reduce fluid temperatures. Given uncertainties in the proximity and intensity of the heat source, the fluid flow rate, and the actual formation temperature of the alteration mineral assemblage, we contend that in situ formation of crystalline, monoclinic tridymite at the Buckskin drill site through hydrothermal processes is a viable alternative to the detrital accumulation of silicic volcanic material.

4. Conclusions

- Interpretation of the tridymite-bearing Buckskin drill sample in the Murray formation as a detrital accumulation of silicic volcanic material (Morris et al., 2016) is puzzling given its low Al_2O_3, high TiO_2, high Ca in the plagioclase feldspar, and absence of any other regions of similar composition encountered along the traverse.
- The average bulk chemical composition of the Murray formation (excluding sulphate-rich samples and ~10 high-silica measurements) over 320 m of elevation is remarkably uniform, including members both above and below the tridymite-bearing drill location. This consistency suggests that the Murray formation is dominated by a single source of sediment and that mineralogical variations largely result from in situ diagenesis with relatively little mobility of major elements.
- The elemental composition of high-silica Murray formation samples (including the tridymite-bearing material) relative to typical Murray composition parallels the differences between the silica-rich alteration halos cross-cutting the Stimson sandstone and the unaltered parent rock. Evolved gas analysis results and isotopic data also indicate that the alteration halos and the Buckskin drill sample interacted with common fluids which did not affect other parts of the Murray formation.
- Cu, Se, Pb and other trace element concentrations as well ferripyrophyllite, saponite, gray hematite, sanidine, cristobalite, anhydrite and other mineral phases found throughout in the Murray formation could be consistent with hydrothermal interactions at a variety of temperatures after deposition of the sediments.
- The mineralogy of the Buckskin sample is consistent with terrestrial fumarolic deposits, and we propose the in situ development of tridymite as an alternative to a detrital accumulation. The temperature of the tridymite formation could have been within its thermodynamic stability field (>870°C) driven by a yet undetected subsurface volcanic heat source. Alternatively, lower formation temperatures may be possible given disequilibrium conditions typical of fumarolic systems as well as indications in terrestrial hydrothermal environments that micron-scale crystalline tridymite domains develop in association with opal-CT.

Data Availability Statement

Archived APXS data are available in tabulated form from the Planetary Data System: https://pds-geosciences.wustl.edu/msl/msl-m-apxs-4_5-rdr-v1/mslapx_1xxx/extras/ (https://doi.org/10.17189/1518757). Specific APXS measurements used in this manuscript are listed in the Supporting Information (Yen et al., 2020; http://doi.org/10.5281/zenodo.4298820).

Acknowledgments
This research was supported by the NASA Mars Science Laboratory Mission. A portion of this work was carried out at the Jet Propulsion Laboratory, California Institute of Technology under a contract with NASA. The authors thank Hap McSween, Edwin Kite, Janice Bishop, and anonymous reviewers whose comments and suggestions improved this manuscript.

References

Abramov, O., & Kring, D. A. (2005). Impact-induced hydrothermal activity on early Mars. *Journal of Geophysical Research*, *110*(E12S09). https://doi.org/10.1029/2005JE002453

Africano, F., Bernard, A., & Korzhinsky, M. (2003). High temperature volcanic gas geochemistry (major and minor elements) at Kudryavy volcano, Iturup Island, Kuril Arc, Russia. *Vulcanica*, *I*, 87–94.

Arnorsson, S. (1984). Germanium in Icelandic geothermal systems. *Geochimica et Cosmochimica Acta*, *48*, 2489–2502.

Auclair, G., Fouquet, Y., & Bohn, M. (1987). Distribution of selenium in high-temperature hydrothermal sulphide deposits at 13-degrees-north, East Pacific Rise. *Canadian Mineralogist*, *25*, 577–587.

Banham, S. G., Gupta, S., Rubin, D. M., Watkins, J. A., Sumner, D. Y., Edgett, K. E., et al. (2018). Ancient martian aeolian processes and paleomorphology reconstructed form the Stimson formation on the lower slope of Aeolis Mons, Gale crater, Mars. *Sedimentology*, *65*, 993–1042. https://doi.org/10.1111/sed.12469

Beaufort, D., Rigault, C., Billon, S., Billault, V., Inoue, A., Inoue, S., & Patrier, P. (2015). Chlorite and chloritization processes through mixed-layer mineral series in low-temperature geological systems – a review. *Clay Minerals*, *50*, 497–523. https://doi.org/10.1180/claymin.2015.050.4.06

Bedford, C. C., Bridges, J. C., Schwenzer, S. P., Wiens, R. C., Rampe, E. B., Frydenvang, J., & Gasda, P. J. (2019). Alteration trends and geochemical source region characteristics preserved in the fluviolacustrine sedimentary record of Gale crater, Mars. *Geochimica et Cosmochimica Acta*, *246*, 234–266. https://doi.org/10.1016/j.gca.2018.11.031

Bell, J. F., III, Godber, A., McNair, S., Caplinger, M. A., Maki, J. N., Lemmon, M. T., et al. (2017). The Mars Science Laboratory Curiosity rover Mastcam instruments: Preflight and in-flight calibration, validation, and data archiving. *Earth and Space Science*, *4*, 396–452. https://doi.org/10.1002/2016EA000219

Berger, J. A., Schmidt, M. E., Gellert, R., Boyd, N. I., Desouza, E. D., Flemming, R. L., et al. (2017). Zinc and germanium in the sedimentary rocks of Gale Crater on Mars indicate hydrothermal enrichment followed by diagenetic fractionation. *Journal of Geophysical Research: Planets*, *122*(8), 1747–1772. https://doi.org/10.1002/2017JE005290

Black, B. A., & Manga, M. (2016). The eruptibility of magmas at Tharsis and Syrtis major on Mars. *Journal of Geophysical Research: Planets*, *121*, 944–964. https://doi.org/10.1002/2016JE004998

Blake, D., Vaniman, D., Achilles, C., Anderson, R., Bish, D., Bristow, T., et al. (2012). Characterization and calibration of the CheMin Mineralogical Instrument on Mars Science Laboratory. *Space Science Reviews*, *170*(1–4), 341–399. https://doi.org/10.1007/s11214-012-9905-1

Borlina, C. S., Ehlmann, B. L., & Kite, E. S. (2015). Modeling the thermal and physical evolution of Mount Sharp's sedimentary rocks, Gale Crater, Mars: Implications for diagenesis on the MSL Curiosity rover traverse. *Journal of Geophysical Research: Planets*, *120*(8), 1396–1414. https://doi.org/10.1002/2015JE004799

Bristow, T. F., Rampe, E. B., Achilles, C. N., Blake, D. F., Chipera, S. J., Craig, P., et al. (2018). Clay mineral diversity and abundance in sedimentary rocks of Gale crater, Mars. *Science Advance*, *4*(6). 1–8. https://doi.org/10.1126/sciadv.aar3330

Cady, S. L., Wenk, H.-R., & Downing, K. H. (1996). HRTEM of microcrystalline opal in chert and porcelanite from the Monterey Formation, California. *American Mineralogist*, *81*, 1380–1395.

Chipera, S. J. & D. L. Bish, 2002. FULLPAT: A full-pattern quantitative analysis program for X-ray powder diffraction using measured and calculated patterns, *Journal of Applied Crystallography*, *35*(6), 744–749. https://doi.org/10.1107/S0021889802017405

Crowe, B. M., Linn, G. W., Heiken, G., & Bevier, M. L. (1978). *Stratigraphy of the Bandelier Tuff in the Pajarito Plateau*. Los Alamos report #LA-7225-MS.US Department of Energy.

Curtis, N. J., Gascooke, J. R., Johnston, M. R., & Pring, A. (2019). A review of the classification of opal with reference to recent new localities. *Minerals*, *9*(5), 299. https://doi.org/10.3390/min9050299

Czarnecki, S., Hardgrove, C., Gasda, P. J., Gabriel, T. S. J., Starr, M., Rice, M. S., et al. (2020). Identification and description of silicic Volcaniclastic layer in Gale crater, Mars, using active Neutron Interrogation. *Journal of Geophysical Research: Planets*, *125*. https://doi.org/10.1029/2019JE006180

Dill, H. G. (2001). The geology of aluminum phosphates and sulphates of the alunite group minerals: A review. *Earth-Science Reviews*, *53*, 35–93. https://doi.org/10.1016/S0012-8252(00)00035-0

Edgett, K. S., Yingst, R. A., Ravine, M. A., Caplinger, M. A., Maki, J. N., Ghaemi, F. T., et al. (2012). Curiosity's Mars Hand Lens imager (MAHLI) Investigation. *Space Science Reviews*, *170*, 259–317. https://doi.org/10.1007/s11214-012-9910-4

Elzea, J. M., Odom, I. E., & Miles, W. J. (1994). Distinguishing well ordered opal-CT and opal-C from high temperature cristobalite by X-ray diffraction. *Analytica Chimica Acta*, *286*, 107–116. https://doi.org/10.1016/0003-2670(94)80182-7

Elzea, J. M., & Rice, S. B. (1996). TEM and X-ray diffraction evidence for cristobalite and tridymite stacking sequences in opal. *Clays Clay Min*, *44*(4), 492–500. https://doi.org/10.1346/CCMN.1996.0440407

Fishman, M. J., & Hem, J. D. (1976).*Lead content of water. Lead in the environment*. USGS professional paper 957. T. G. Lovering.

Franz, H. B., Mahaffy, P. R., Webster, C. R., Flesch, G. J., Raaen, E., Freissinet, C., et al. (2020). Indigenous and exogenous organics and surface-atmosphere cycling inferred from carbon and oxygen isotopes at Gale crater. *Nature Astronomy*, *4*(5), 526. https://doi.org/10.1038/s41550-019-0990-x

Franz, H. B., McAdam, A. C., Ming, D. W., Freissinet, C., Mahaffy, P. R., Eldridge, D. L., et al. (2017). Large sulfur isotope fractionations in Martian sediments at Gale crater. *Nature Geoscience*, *10*(9). 658–663. https://doi.org/10.1038/NGEO3002

Frydenvang, J., Gasda, P. J., Hurowitz, J. A., Grotzinger, J. P., Wiens, R. C., Newsom, H. E., et al. (2017). Diagenetic silica enrichment and late-stage groundwater activity in Gale crater, Mars. *Geophysical Research Letters*, *44*, 1–9. https://doi.org/10.1002/2017GL073323

Ganino, C., Libourel, G., & Bernard, A. (2019). Fumarolic incrustations at Kudryavy volcano (Kamchatka) as a guideline for high-temperature (>850°C) extinct hydrothermal systems. *Journal of Volcanology and Geothermal Research*, *376*, 75–85. https://doi.org/10.1016/j.jvolgeores.2019.03.020

Gellert, R., & Yen, A. S. (2019). Elemental analyses of Mars from rovers using the Alpha-Particle X-ray spectrometer. In J. L. Bishop, J. F. BellIII, & J. E. Moersch (Eds.), *Remote Compositional Analysis*. Cambridge University Press.

Getahun, A., Reed, M. H., & Symonds, R. (1996). Mount St. Augustine volcano fumarole wall rock alteration: Mineralogy, zoning, composition and numerical models of its formation process. *Journal of Volcanology and Geothermal Research*, *71*, 73–107.

Ghisoli, C., Caucia, F., & Marinoni, L. (2010). XRPD patterns of opals: A brief review and new results from recent studies. *Powder Diffraction*, *25*(3), 274–282. https://doi.org/10.1154/1.3478554

Giardini, D., Lognonne, P., Banerdt, W. B., Pike, W. T., Christensen, U., Cylan, S., et al. (2020). The seismicity of Mars. *Nature Geoscience*, *13*, 205–212. https://doi.org/10.1038/s41561-020-0539-8

Grotzinger, J. P., Gupta, S., Malin, M. C., Rubin, D. M., Schieber, J., Siebach, K. et al. (2015). Deposition, exhumation, and paleoclimate of an ancient lake deposit, Gale crater, Mars. *Science*, *350*(6257), aac7575–aac7575-12. https://doi.org/10.1126/science.aac7575

Guthrie, G. D., Jr., Bish, D. L., & Reynolds, R. C., Jr. (1995). Modeling the X-ray diffraction pattern of opal-CT. *American Mineralogist*, *80*, 869–872.

Hamasaki, S. (2002). Volcanic-related alteration and geochemistry of Iwodake volcano, Satsuma-Iwojima, Kyushu, SW Japan. *Earth Planets and Space*, *54*(3), 217–229. https://doi.org/10.1186/BF03353021

Hannington, M., Herzig, P., Stoffers, P., Scholten, J., Botz, R., Garbe–Schönberg, D., et al. (2001). First observations of high-temperature submarine hydrothermal vents and massive anhydrite deposits off the north coast of Iceland. *Marine Geology*, *177*(3–4), 199–220. https://doi.org/10.1016/S0025-3227(01)00172-4

Hausrath, E. M., Ming, D. W., Peretyazhko, T. S., & Rampe, E. B. (2018). Reactive transport and mass balance modeling of the Stimson sedimentary formation and altered fracture zones constrain diagenetic conditions at Gale crater, Mars. *EPSL*, *491*, 1–10. https://doi.org/10.1016/j.epsl.2018.02.037

Heaney, P. J. (1994). Structure and Chemistry of the low-pressure silica polymorphs. *Reviews in Mineralogy*, *29*, 1–40.

Hicks, L. J., Bridges, J. C., & Gurman, S. J. (2014). Ferric saponite and serpentine in the nakhlite martian meteorites. *Geochimica et Cosmochimica Acta*, *136*, 194–210. http://dx.doi.org/10.1016/j.gca.2014.04.010

Hillier, S., & Lumsdon, D. G. (2008). Distinguishing opaline silica from cristobalite in bentonites: A practical procedure and perspective based on NaOH dissolution. *Clay Minerals*, *43*, 477–486. https://doi.org/10.1180/claymin.2008.043.3.11

Hynek, B. M., McCollom, T. M., Marcucci, E. C., Brugman, K., & Rogers, K. L. (2013). Assessment of environmental controls on acid-sulphate alteration at active volcanoes in Nicaragua: Applications to relic hydrothermal systems on Mars. *Journal of Geophysical Research: Planets*, *118*, 2083–2104. https://doi.org/10.1002/jgre.20140

Ilieva, A., Mihailova, B., Tsintsov, Z., & Petrov, O. (2007). Structural state of microcrystalline opals: A Raman spectroscopic study. *American Mineralogist*, *92*, 1325–1333. https://doi.org/10.2138/am.2007.2482

Jackson, J. C., Horton, J. W., Jr., Chou, I.-M., & Belkin, H. E. (2011). Monoclinic tridymite in clast-rich impact melt rock from the Chesapeake Bay impact structure. *American Mineralogist*, *96*, 81–88. https://doi.org/10.2138/am.2011.3589

Jones, J. B., & Segnit, E. R. (1972). Genesis of cristobalite and tridymite at low temperatures. *Journal of the Geological Society of Australia*, *18*(4), 419–422. https://doi.org/10.1080/00167617208728780

Kihara, K., Matsumoto, T., & Imamura, M. (1986). Structural change of orthorhombic-I tridymite with temperature: A study based on second-order thermal-vibrational parameters. *Zietschrift für Kristallographie*, *177*(1–2), 27–38. https://doi.org/10.1524/zkri.1986.177.1-2.27

Kite, E. S., Halevy, I., Kahre, M. A., Wolff, M. J., & Manga, M. (2013b). Seasonal melting and the formation of sedimentary rocks on Mars, with predictions for the Gale crater mound. *Icarus*, *223*, 181–210. https://doi.org/10.1016/j.icarus2012.11.034

Kite, E. S., Lewis, K. W., Lamb, M. P., Newman, C. E., & Richardson, M. I. (2013a). Growth and form of the mound in Gale Crater, Mars: Slope wind enhanced erosion and transport. *Geology*, *41*(5), 543–546. https://doi.org/10.1130/G33909

Klasik, J. A. (1975). High cristobalite and high tridymite in a middle Eocene deep-sea chert. *Science*, *189*(4203), 631–632. https://doi.org/10.1126/science.189.4203.631

Komatsu, G., Ishimaru, R., Miyake, N., Kawai, K., Kobayashi, M., Sakuma, H., & Matsui, T. (2019). The Goshogake mud volcano field, Tohoku, northern Japan: An acidic, high-temperature system related to magmatic volcanism. *Geomorphology*, *329*, 32–45. https://doi.org/10.1016/j.geomorph.2018.12.035

Kring, D. A., Tikoo, S. M., Schmieder, M., Riller, U., Rebolledo-Vieyra, M., Simpson, S. L., et al. (2020). Probing the hydrothermal system of the Chicxulub impact crater. *Science Advance*, *6*, 1–9. https://doi.org/10.1126/sciadv.aaz3053

Krivovichev, V. G., Charykova, M. V., & Vishnevsky, A. V. (2017). The thermodynamics of selenium minerals in near-surface environments. *Minerals*, *7*(10), 1–18. https://doi.org/10.3390/min7100188

Lee, S., & Xu, H. (2019). Using powder XRD and pair distribution function to determine anisotropic atomic displacement parameters of orthorhombic tridymite and tetragonal cristobalite. *Acta Cryst*, *B75*, 1–17. https://doi.org/10.1107/S2052520619000933

Lewis, K. W., Peters, S., Gonter, K., Morrison, S., Schmerr, N., Vasavada, A. R., &(2019). A surface gravity traverse on Mars indicates low bedrock density at Gale crater. *Science*, *363*, 535–537. https://doi.org/10.1126/science.aat0738

Liu, W., & McPhail, D. C. (2005). Thermodynamic properties of copper chloride complexes and copper transport in magmatic-hydrothermal solutions. *Chemical Geology*, *221*, 21–39. https://doi.org/10.1016/j.chemgeo.2005.04.009

Mahaffy, P. R., Webster, C. R., Cabane, M., Conrad, P. G., Coll, P., Atreya, S. K., et al. (2012). The Sample Analysis at Mars Investigation and instrument suite. *Space Science Reviews*, *170*(1–4), 401–478. https://doi.org/10.1007/s11214-012-9879-z

Martin, P. E., Farley, K. A., Malespin, C. A., Schwenzer, S. P., Cohen, B. A., et al. (2017). A two-Step K-Ar experiment on Mars: Dating the diagenetic formation of Jarosite from Amazonian Groundwaters. *Journal of Geophysical Research: Planets*, *122*(12), 2803–2818. https://doi.org/10.1002/2017JE005445

Morris, R. V., Rampe, E. B., Vaniman, D. T., Christoffersen, R., Yen., A. S., Morrison, S. M., et al. (2020). Hydrothermal precipitation of sanidine (Adularia) having extreme Al, Si structural disorder and Specular hematite at the Maunakea hematite ridge (Hawaii) and at Gale crater (Mars). *Journal of Geophysical Research: Planets*. https://doi.org/10.1029/2019JE006324

Morris, R. V., Vaniman, D. T., Blake, D. F., Gellert, R., Chipera, S. J., Rampe, E. B., et al. (2016). Silicic volcanism on Mars evidenced by tridymite in high-SiO_2 sedimentary rock at Gale crater. *Proceedings of the National Academy of Sciences*, *113*(26), 7071–7076. https://doi.org/10.1073/pnas.1607098113

Morrison, S. M., Downs, R. T., Blake, D. F., Vaniman, D. T., Ming, D. W., Hazen, R. M., et al. (2018). Crystal chemistry of martian minerals from Bradbury landing through Naukluft plateau, Gale crater, Mars. *American Mineralogist*, *103*, 857–871. https://doi.org/10.2138/am-2018-6124

Nachon, M., Mangold, N., Forni, O., Kah, L. C., Cousin, A., Wiens, R. C., et al. (2017). Chemistry of diagenetic features analyzed by ChemCam at Pahrump Hills, Gale crater, Mars. *Icarus*, *281*, 121–136. https://doi.org/10.1016/j.icarus.2016.06.026

Ostrooumov, M. (2007). A Raman, infrared and XRD analysis of the instability in volcanic opals from Mexico. *Spectrochimica Acta*, *68*, 1070–1076. https://doi.org/10.1016/j.saa.2007.06.048

Plescia, J. B. (1990). Recent flood lavas in the Elysium region of Mars. *Icarus*, *88*, 465–490. https://doi.org/10.1016/j.saa.2007.06.048

Pokrovski, G. S., & Schott, J. (1998). Thermodynamic properties of aqueous Ge(IV) hydroxide complexes from 25 to 350°C: Implications for the behavior of germanium and the Ge/Si ratio in hydrothermal fluids. *Geochimica et Cosmochimica Acta*, *62*(9), 1631–1642. https://doi.org/10.1016/S0016-7037(98)00081-7

Rampe, E. B., Bristow, T. F., Morris, R. V., Morrison, S. M., Achilles, C. N., Ming, D. W., et al. (2020). Mineralogy of the Vera Rubin Ridge from the Mars Science laboratory CheMin instrument. *Journal of Geophysical Research: Planets*, *125*. https://doi.org/10.1029/2019JE006306

Rampe, E. B., Ming, D. W., Blake, D. F., Bristow, T. F., Chipera, S. J., Grotzinger, J. P., et al. (2017). Mineralogy of an ancient lacustrine mudstone succession from the Murray formation, Gale crater, Mars, *EPSL*, *471*, 172–185. https://doi.org/10.1016/j.epsl.2017.04.021

Rapin, W., Chauvire, B., Gabriel, T. S. J., McAdam, A. C., Ehlmann, B. L., Hardgrove, C., et al. (2018). In situ analysis of opal in Gale crater, Mars. *Journal of Geophysical Research*, *123*, 1955–1972. https://doi.org/10.1029/2017JE005483

Rapin, W., Meslin, P.-Y., Maurice, S., Vaniman, D., Nachon, M., Mangold, N., et al. (2016). Hydration state of calcium sulfates in Gale crater, Mars. Identification of bassanite veins. *EPSL*, *452*, 197–205. https://doi.org/10.1016/j.epsl.2016.07.045

Reyes, A. G. (1990). Petrology of Philippine geothermal systems and the application of alteration mineralogy to their assessment. *Journal of Volcanology and Geothermal Research*, *43*, 279–309.

Schwenzer, S. P., Abramov, O., Allen, C. C., Bridges, J. C., Clifford, S. M., Filiberto, J., et al. (2012). Gale Crater: Formation and post-impact hydrous environments. *Planetary and Space Science*, *70*, 84–95. https://doi.org/10.1016/j.pss.2012.05.014

Stillings, L. L. (2017). *Selenium, Chapter Q of Critical mineral resources of the United States—economic and environmental geology and prospects for future supply*, USGS Professional Paper 1802-Q. US Geological Survey.

Sutter, B., McAdam, A. C., Mahaffy, P. R., Ming, D. W., Edgett, K. S., Rampe, E. B., et al. (2017). Evolved gas analyses of sedimentary rocks and eolian sediment in Gale Crater, Mars: Results of the Curiosity rover's sample analysis at Mars instrument from Yellowknife Bay to the Namib Dune. *Journal of Geophysical Research: Planets*, *122*. https://doi.org/10.1002/2016JE005225

Tada, R., & Iijima, A. (1982). Identification of mixtures of opaline silica phases and its implication for silica diagenesis. *Developments in Sedimentology*, *36*, 229–245.

Vaniman, D. T., Bish, D. L., Ming, D. W., Bristow, T. F., Morris, R. V., Blake, D. F., et al. (2014). Mineralogy of a mudstone at Yellowknife Bay, Gale crater, Mars. *Science*, *343*(6169), 1243480-1–1243480-8. https://doi.org/10.1126/science.1243480

Vaniman, D. T., Martinez, G. M., Rampe, E. B., Bristow, T. F., Blake, D. F., Yen, A. S., et al. (2018). Gypsum, bassanite, and anhydrite at Gale crater, Mars. *American Mineralogist*, *103*(7), 1011–1020. https://doi.org/10.2138/am-2018-6346

Wang, Y., Han, X., Petersen, S., Frische, M., Qiu, Z., Li, H., et al. (2017). Mineralogy and trace element geochemistry of sulfide minerals from the Wocan hydrothermal field on the slow-spreading Carlsberg ridge, Indian ocean. *Geology Reviews*, *84*, 1–19. https://doi.org/10.1016/j.oregeorev.2016.12.020

Wiens, R. C., Maurice, S., Barraclough, B., Saccoccio, M., Barkley, W. C., Bell, J. F., III, et al. (2012). The ChemCam instrument suite on the Mars Science Laboratory (MSL) rover: Body Unit and Combined system Tests. *Space Science Reviews*, *170*, 167–227. https://doi.org/10.1007/s11214-012-9902-4

Williams, R. M. E., Sumner, D. Y., Gupta, S., Grotzinger, J. P., Rubin, D., Wiens, R. C., et al. (2014). *Sedimentology of Darwin waypoint from curiosity observations*. 45th LPSC, #2401. Lunar and Planetary Institute.

Wilson, M. J. (2014). The structure of opal-CT revisited. *Journal of Non-crystalline Solids*, *405*, 68–75. https://doi.org/10.1016/j.jnoncrysol.2014.08.052

Yen, A. S., Ming, D. W., Vaniman, D. T., Gellert, R., Blake, D. F., Morris, R. V., et al. (2017). Multiple stages of aqueous alteration along fractures in mudstone and sandstone strata in Gale Crater, Mars. *EPSL*, *471*, 186–198. https://doi.org/10.1016/j.epsl.2017.04.033

Yen, A. S., Morris, R. V., Ming, D. W., Schwenzer, S. P., Sutter, B., Vaniman, D. T., et al. (2020). *Supporting information for Yen et al. "Formation of Tridymite and Evidence for a Hydrothermal History at Gale Crater, Mars*. AGU/JGR-Planets. http://doi.org/10.5281/zenodo.4298820

Zimbelman, D. R., Rye, R. O., & Breit, G. N. (2005). Origin of secondary sulphate minerals on active andesitic stratovolcanoes. *Chemical Geology*, *215*, 37–60. https://doi.org/10.1016/j.chemgeo.2004.06.056

Reference From the Supporting Information

Nesbit, H. W. (1979). Mobility and fractionation of rare earth elements during weathering of a granodiorite. *Nature*, *279*, 206–210.